Thermochimica Acta, 51 (1981) 245–267
Elsevier Scientific Publishing Company, Amsterdam—Printed in Belgium

EFFECT OF α-Fe_2O_3 ADDITIVE ON THE THERMAL DECOMPOSITION OF SALTS OF HALOGEN OXOACIDS, OXALATES, AZIDE, PERMANGANATE, AND OXIDES

RYUSABURO FURUICHI, TADAO ISHII, ZENZO YAMANAKA and MASAHIDE SHIMOKAWABE

Department of Applied Chemistry, Faculty of Engineering, Hokkaido University, 060 Sapporo (Japan)

(Received 20 May 1981)

ABSTRACT

The effect of additives on the thermal decomposition of salts of halogen oxoacids ($KClO_4$, $KClO_3$, KIO_4 and $KBrO_3$), oxalates ($NiC_2O_4 \cdot 2H_2O$, $MgC_2O_4 \cdot 2H_2O$ and $CaC_2O_4 \cdot H_2O$), azide (NaN_3), permanganate ($KMnO_4$), and oxides (MnO_2 and PbO_2) was studied by gas-flow type DTA and X-ray diffraction of samples obtained in the course of the decomposition. α-Fe_2O_3 was mainly employed as the additive, which was prepared from $FeC_2O_4 \cdot 2H_2O$ by calcining it in flowing air (100 ml min^{-1}) at 500°C. α-Al_2O_3, CuO, Cu_2O and NiO were also tested as additives in a few cases. DTA experiments were carried out in static air, flowing N_2 and O_2 (50 ml min^{-1}) at a heating rate of 5°C min^{-1}.

The additive α-Fe_2O_3 exhibited a remarkable catalytic acceleration effect on the decomposition of salts of halogen oxoacids. For the decomposition reactions of other substances, α-Fe_2O_3 did not show the effects detectable with DTA technique. However, it was observed by X-ray analysis that α-Fe_2O_3 reacted to form $MgFe_2O_4$ and $CaFe_2O_4$ for oxalates, $PbFe_2O_4$ for PbO_2, and an unknown compound for $KMnO_4$.

INTRODUCTION

It has been shown in many works that the mechanical addition of a foreign substance to metallic salts gives rise to changes in the thermochemical reaction behavior of the salts [1–13]. The changes may be due to (i) the chemical reaction occurring between reactant and additive to form some stable compounds [1–8], and (ii) the catalytic action of additive accelerating or decelerating the reaction [9–13]. DTA technique gives extensive information on the reaction behavior covering a wide temperature range by only one experimental run. In the present study, DTA technique was employed as a screening test together with X-ray technique to determine the effect of additive on the thermal decomposition of salts of halogen oxoacids ($KClO_4$, $KClO_3$, KIO_4 and $KBrO_3$), oxalates ($NiC_2O_4 \cdot 2H_2O$, $MgC_2O_4 \cdot 2H_2O$, and $CaC_2O_4 \cdot H_2O$), azide (NaN_3), permanganate ($KMnO_4$), and oxides (MnO_2 and PbO_2). Ferric oxide (α-Fe_2O_3) was mainly used as the additive, and α-Al_2O_3, CuO, Cu_2O and NiO were also examined in some experiments.

0040-6031/81/0000–0000/$02.75

EXPERIMENTAL

Materials

Additives

α-Fe_2O_3. Ferric oxide was prepared from $FeC_2O_4 \cdot 2H_2O$ by calcining it in flowing air (100 ml min^{-1}) at 500°C for 1 h. The oxide obtained was ground to pass through 200 mesh sieve and then subjected to X-ray diffraction for identification as α-Fe_2O_3 (ASTM 13-534).

α-Al_2O_3. Activated alumina (Merck) was heated in static air at 1300°C for 3 h. The alumina powders passed through 200 mesh sieve were used as additive and the reference material of DTA experiments.

CuO. Commercial reagent.

Cu_2O. Copper(I) oxide was obtained from CuO by calcining it in flowing N_2 (300 ml min^{-1}) at 900°C for 3 h. The X-ray diffraction pattern of the oxide agreed with ASTM 5-0667.

NiO. Thermal decomposition of $NiCO_3 \cdot 2Ni(OH)_2 \cdot 4H_2O$ was carried out in static air at 1000°C for 4 h. The resultant material was confirmed to be NiO (ASTM 4-0835).

Samples

All samples, $KClO_4$, $KClO_3$, KIO_4, $KBrO_3$, $NiC_2O_4 \cdot 2H_2O$, $MgC_2O_4 \cdot 2H_2O$, $CaC_2O_4 \cdot H_2O$, NaN_3, $KMnO_4$, MnO_2, and PbO_2, were commercial reagents from Kanto Chem. Co. and used for the experiments without purification. The mixing ratio of sample to additive was 1 : 1 (by wt.) except for KIO_4 (1 : 4) and NaN_3 (1 : 5). Mixing was carried out in an agate mortar for 30 min. In the case without additive, the pure sample was also ground for 30 min.

DTA

The laboratory apparatus and procedures have been previously reported in detail [7]. The apparatus consists of two quartz tubes (inner diameter 10 mm) placed vertically in an electric furnace, through which any kind of gas stream can be passed. The sample packed in the quartz tube can be quenched rapidly with cold water to stop the reaction. The experimental conditions were as follows; weight of sample and reference material (α-Al_2O_3) = 1 g, heating rate = 5°C min^{-1}, and thermocouple = chromel–alumel, 0.3 mm diameter. Nitrogen and oxygen gas (Hokusan Co.) were passed through a dryer (silica gel) and flow meter before entering the DTA apparatus.

X-Ray diffraction

X-Ray diffraction was carried out using Geigerflex type 2141 and 2001 (Rigaku Denki Co.) diffractometers equipped with a Cu and Co X-ray tube. The sample for X-ray analysis was obtained by quenching in the DTA quartz tube to room temperature from various temperatures in the course of the reaction.

RESULTS AND DISCUSSION

Salts of halogen oxoacids ($KClO_4$, $KClO_3$, KIO_4 and $KBrO_3$)

Figure 1 shows the DTA results of $KClO_4$, $KClO_3$ and those containing α-Al_2O_3 and α-Fe_2O_3 measured in static air. Details of these results have been reported previously [1,9,10]. The endothermic peak at 310°C on curves 1–3 is due to the

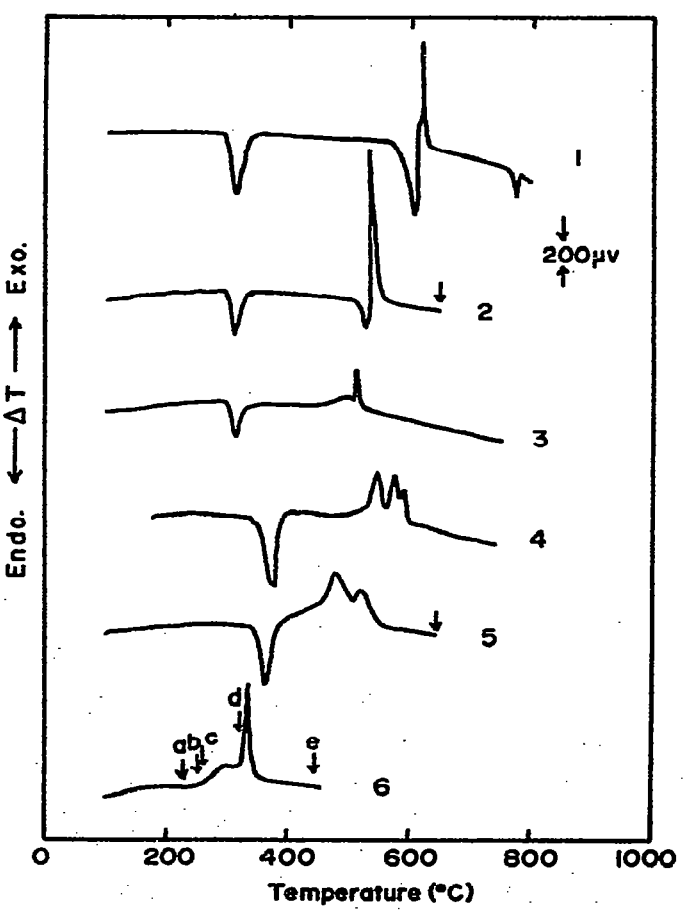

Fig. 1. DTA curves of $KClO_4$ and $KClO_3$ systems in static air. (1) $KClO_4$, (2) $KClO_4+\alpha$-Al_2O_3, (3) $KClO_4+\alpha$-Fe_2O_3, (4) $KClO_3$, (5) $KClO_3+\alpha$-Al_2O_3, (6) $KClO_3+\alpha$-Fe_2O_3. Heating rate=5°C min^{-1}; mixing ratio of sample to additive=1:1 by weight. Arrows on the curves show temperatures at which the samples were obtained for X-ray diffraction.

reversible crystallographic transformation of $KClO_4$. The additives (α-Al_2O_3 and α-Fe_2O_3) are found to give no effect on the transformation process. After the crystallographic transformation, pure $KClO_4$ (curve 1) shows two endothermic peaks at 605 and 780°C, and a sharp exothermic peak at 615°C. The endothermic peaks correspond to fusion of $KClO_4$ and KCl [14], respectively. The exothermic peak is due to the decomposition of $KClO_4$ to KCl in the molten state [9,10]. As seen from curve 2, α-Al_2O_3 additive results in a similar DTA pattern to that of pure $KClO_4$. However, the peak temperatures of the fusion and the decomposition in the molten state in $KClO_4$–α-Al_2O_3 mixture are 525 and 535°C, respectively, which are lower by about 80°C than those of $KClO_4$ alone. At 650°C, after the decomposition (arrow on curve 2), X-ray diffraction showed the existence of KCl and α-Al_2O_3. After the crystallographic transformation, the α-Fe_2O_3–$KClO_4$ mixture (curve 3) gives a broad exothermic deflection starting at 450°C, with its peak at 495°C which is followed by a small sharp exothermic peak at 510°C. The broad exothermic deflection is due to the decomposition of $KClO_4$ in the solid state before fusion and the sharp one is due to the decomposition in the molten state [9,10,15,16]. As mentioned above, α-Fe_2O_3 indicates the remarkable acceleration effect on the decomposition, but no chemical reactions between the oxide and perchlorate were detected by X-ray analysis [9,10].

Figure 1 (curves 4–6) show the DTA results of $KClO_3$ in static air. The endothermic peak at 375°C on curve 4 corresponds to melting of pure $KClO_3$ [1,16,17]. The exothermic peak with the fine structure appears between 500 and 600°C, which results from the decomposition of $KClO_3$ in the molten state. This fine structure suggests that the decomposition proceeds through multi-reaction steps. Rudloff and Freeman [16,17] assumed the following process

$$2\ KClO_3 \rightarrow KClO_4 + KCl + O_2, \quad \Delta H_{627°C} = -105\ \text{kJ mole}^{-1} \tag{1}$$

$$KClO_4 \rightarrow KCl + 2\ O_2, \quad \Delta H_{627°C} = -54\ \text{kJ mole}^{-1} \tag{2}$$

Markowitz et al. [18] proposed eqns. (3) and (4) for eqn. (1)

$$KClO_3 \rightarrow KCl + 1.5\ O_2 \tag{3}$$

$$KClO_3 \rightarrow 0.75\ KClO_4 + 0.25\ KCl \tag{4}$$

[2 × eqn. (3) + 4 × eqn. (4) = 3 × eqn. (1)].

As seen from curves 4 and 5, the addition of α-Al_2O_3 results in a similar pattern of the DTA curve to pure $KClO_3$, but the peak temperature is shifted to a lower temperature region, from 375 to 365°C for fusion and from 500–600°C to 450–550°C for the exothermic decomposition. KCl and α-Al_2O_3 were present in the sample taken out at 645°C. In the case of α-Fe_2O_3 additive (curve 6), the endothermic peak of fusion disappears and two exothermic peaks (292 and 334°C) appear in the temperature range 250–350°C.

Figure 2 shows X-ray diffraction patterns of samples obtained in the course of the decomposition after having been heated up to temperatures shown by arrows (a–e) in Fig. 1 (curve 6). The decomposition product KCl ($2\theta = 33.0°$) is first observed at 260°C (Fig. 2-c). This temperature coincides with the starting temperature of exothermic deflection due to the start of thermal decomposition of $KClO_3$. In Fig. 2,

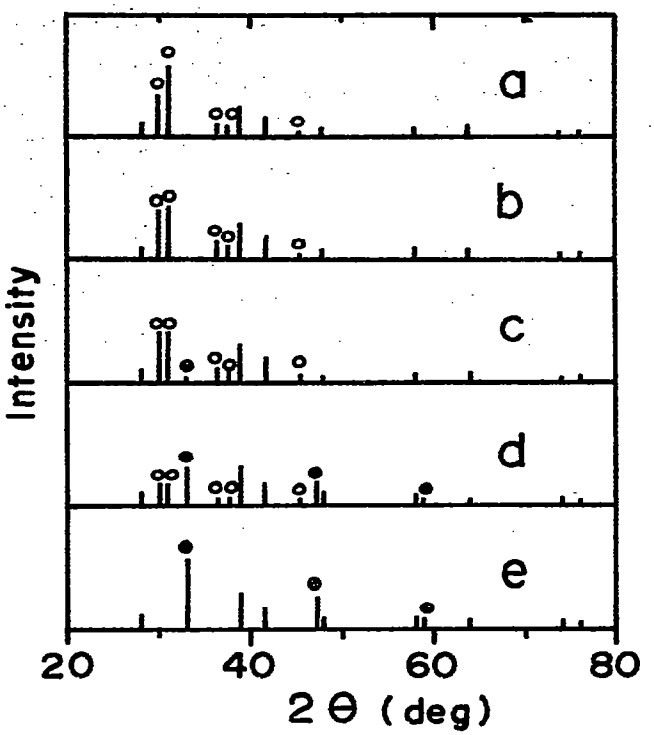

Fig. 2. X-Ray diffraction results of $KClO_3$–α-Fe_2O_3 mixture in the course of the decomposition shown in Fig. 1 (curve 6). (a) 229°C, (b) 255°C, (c) 260°C, (d) 320°C, (e) 445°C. (○) $KClO_3$, (●) KCl, (no mark) α-Fe_2O_3, (2θ) CoK_α.

it is observed that the intensity of the diffraction lines of $KClO_3$ decreases with increasing temperature, in contrast to that of KCl, and at 445°C (Fig. 2-e) only the lines of KCl (and α-Fe_2O_3) are present instead of the absence of $KClO_3$; however, the intensity of the diffraction lines of α-Fe_2O_3 remains unchanged during the decomposition reaction. The results in Fig. 2 also show no formation of the intermediate product $KClO_4$ assumed in eqn. (1) or (4). Wydeven [19] obtained a DTA curve in the case of the $NaClO_3$–Co_3O_4 system similar to that shown in Fig. 1 (curve 6) and concluded that a 60% part of the chlorate decomposes in the solid state, but he gives no description for the intermediate. Solymosi and Krix [20] have reported that NiO mixed with $KClO_3$ selectively catalyzes the reaction of eqn. (3) and other oxides, such as MgO, TiO_2 and ZnO, tend to retard the formation of $KClO_4$ intermediate. These results suggest that the addition of α-Fe_2O_3 to $KClO_3$ gives rise to a similar decomposition process to that of $KClO_4$; that is, the broad exotherm at 292°C corresponds to the solid state decomposition of $KClO_3$ and the sharp exotherm at 334°C is due to the molten state decomposition, represented by eqn. (3). Recently, Rudloff and Freeman [21] showed in the DTA study on Fe_2O_3–$KClO_3$ system that only the exothermic peak of the molten phase decomposition of $KClO_3$ appears after the fusion endothermic peak at 350–400°C. This seems to be the result of the different preparation histories of Fe_2O_3 from the present

experiments [10–12]. Rudloff used the oxide prepared at temperatures higher than 700°C.

DTA curves for KIO_4 measured in static air are shown in Fig. 3 (curves 1–3). No DTA curve of KIO_4 has been reported. Phillip and Taylor [22] investigated the kinetics of the isothermal decomposition of the periodate between 256 and 288°C

$$2\,KIO_4 \rightarrow 2\,KIO_3 + O_2 \qquad (5)$$

Mellor [23] states that the solid KIO_4 does not change at 200°C, but at 300°C it loses oxygen and forms the iodate, and when calcined at a higher temperature it forms the iodide. Figure 4 gives the X-ray diffraction patterns of samples obtained in

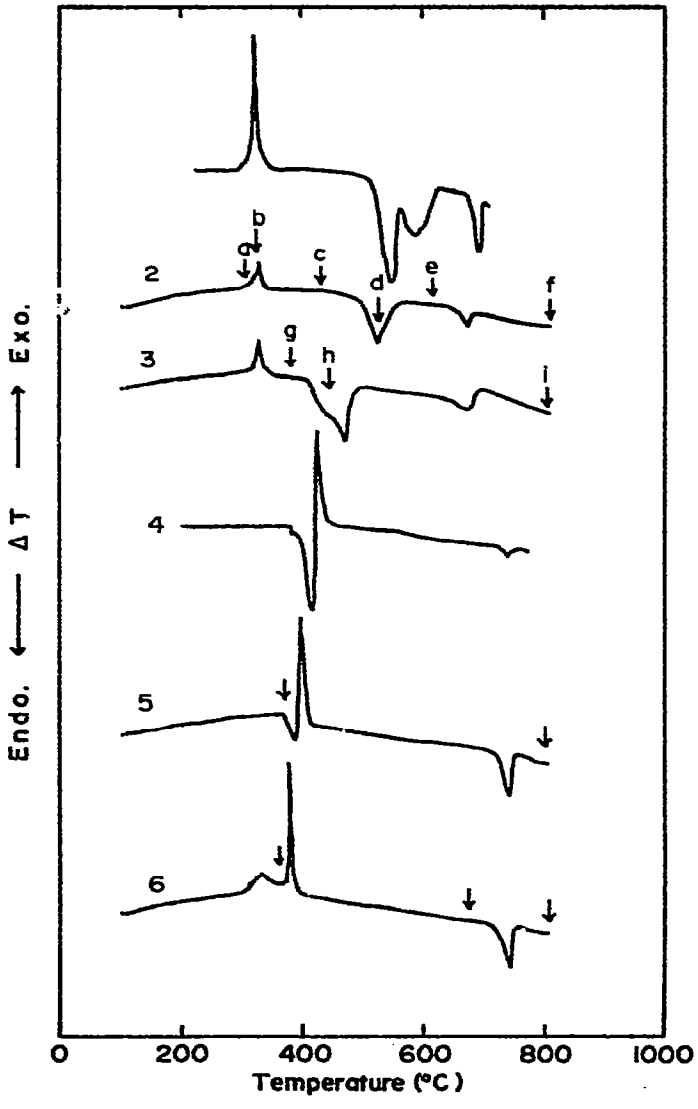

Fig. 3. DTA curves of KIO_4 and $KBrO_3$ systems in static air. (1) KIO_4, (2) $KIO_4 + \alpha\text{-}Al_2O_3$, (3) $KIO_4 + \alpha\text{-}Fe_2O_3$, (4) $KBrO_3$, (5) $KBrO_3 + \alpha\text{-}Al_2O_3$, (6) $KBrO_3 + \alpha\text{-}Fe_2O_3$. Heating rate = 5°C min^{-1}; mixing ratio of sample to additive = 1 : 4 for KIO_4 and 1 : 1 for $KBrO_3$ by weight. Arrows on the curves show temperatures at which the samples were obtained for X-ray diffraction.

the course of decomposition at temperatures shown by arrows (a–i) in Fig. 3 (curves 2 and 3). Curves 1–3 show the exothermic peak at 325°C, on which the addition effect of α-Al_2O_3 and α-Fe_2O_3 is not observed. This exothermic peak is found to correspond to eqn. (5) from X-ray results in Fig. 4-a, b, c and g. Phillips and Taylor [22] have estimated $\Delta H = -209$ kJ mole^{-1} for eqn. (5). The endothermic peak seen at 650–700°C on curves 1–3 is considered to result from melting of KI on the basis of the fact that X-ray analysis of Fig. 4-e and f shows the existence of only KI before and after the endothermic peak and the melting point of pure KI is 686°C reported in ref. [14]. α-Al_2O_3 and α-Fe_2O_3 decrease the melting endother-

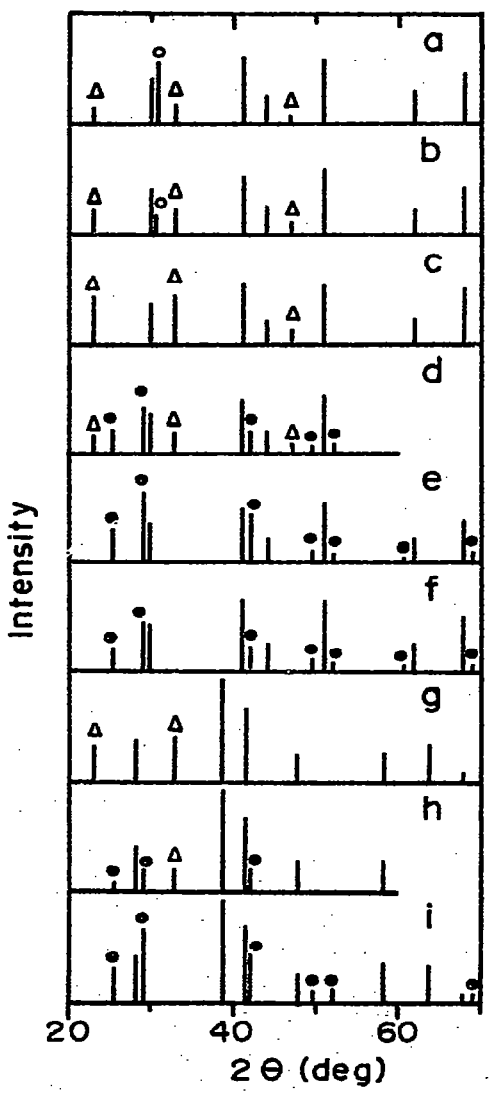

Fig. 4. X-Ray diffraction results of KIO_4–α-Al_2O_3 (a–f) and α-Fe_2O_3 (g–i) mixtures in the course of the decomposition shown in Fig. 3 (curves 2 and 3). (a) 305°C, (b) 320°C, (c) 430°C, (d) 525°C, (e) 615°C, (f) 808°C, (g) 380°C, (h) 445°C, (i) 805°C. (○) KIO_4, (△) KIO_3, (●) KI, (no mark) α-Al_2O_3 or α-Fe_2O_3, (2θ) CoK_α.

mic peak temperature by about 20°C compared with pure KI, as seen in DTA curves 1–3. The X-ray results of Fig. 4-c, d, e, g, and h suggest the decomposition of KIO_3 to KI; therefore the endothermic peaks at 480–560°C on curve 2 and at 410–500°C on curve 3 in Fig. 3 correspond to the decomposition

$$2\ KIO_3 \rightarrow 2\ KI + 3\ O_2 \quad (6)$$

In the case of curve 1, the two endothermic peaks appearing at 550 and 590°C also correspond to the decomposition of KIO_3, but it is not possible at present to show exactly what reactions are assigned to these endothermic peaks. KIO_3 is reported to melt at 560°C [14]. The evolution of a violet colored gas was recognized at about 560°C or above in the case of the decomposition of pure KIO_4 (curve 1). It is considered that the formation of I_2 gas occurs according to eqn. (7) from an analogy to the decomposition of $LiClO_3$ [18]

$$4\ KIO_3 \rightarrow 2\ K_2O + 2\ I_2 + 5\ O_2 \quad (7)$$

Accordingly, it is assumed that two endothermic peaks at 500–650°C in Fig. 3 (curve 1) contain the heat of reaction of eqn. (7) and of melting of KIO_3 in addition to that of eqn. (6). As mentioned above, the addition of α-Fe_2O_3 (curve 3) starts the decomposition [eqn. (6)] at 410°C. Since this starting temperature is lower by about 150°C than the reported melting temperature of KIO_3 (560°C) [14], it is suggested that the decomposition of KIO_3 begins in the solid state and the endothermic melting results in an increase in decomposition rate leading to a sharp endothermic peak at 470°C. It is concluded that the effects of additives are exerted on the reaction of eqn. (6), but not on eqn. (5).

Figure 3 (curves 4–6) show DTA curves of $KBrO_3$ measured in static air. The stoichiometric overall reaction for the bromate [eqn. (8)] is the same as that for the chlorate and iodate [23]

$$2\ KBrO_3 \rightarrow 2\ KBr + 3\ O_2 \quad (8)$$

The melting points of $KBrO_3$ and KBr are 434 and 730°C [14], respectively. Accordingly, on DTA curve 4 of pure $KBrO_3$, the sharp endothermic peak at 415°C may correspond to melting of $KBrO_3$, the sharp exothermic peak at 425°C to the decomposition [eqn. (8)] in the liquid phase, and the small endothermic peak at 740°C to melting of KBr. The melting of KBr does not seem to be affected by the additives (curves 5 and 6). For the mixture $KBrO_3$–α-Al_2O_3 (curve 5), X-ray diffraction of samples taken out at 370 and 800°C showed the presence of $KBrO_3$, KBr (weak intensity of diffraction lines) and α-Al_2O_3 at the low temperature, and KBr and α-Al_2O_3 at the high temperature. The endothermic DTA peak due to melting of the $KBrO_3$–α-Al_2O_3 mixture sets in at 370°C where KBr was detected by X-ray; therefore α-Al_2O_3 seems to promote the solid state decomposition of the bromate before it melts. In the case of α-Fe_2O_3 (curve 6), a broad exothermic peak begins to appear around 260°C and the X-ray diffraction result for the sample obtained at 360°C showed the diffraction lines of $KBrO_3$, KBr and α-Fe_2O_3. These facts may indicate that the broad exothermic peak corresponds to the solid state decomposition of $KBrO_3$. X-Ray results showed KBr and α-Fe_2O_3 for both samples

obtained at 675 and 805°C, which confirm the melting endothermic peak of KBr at 740°C. As seen from Figs. 1 and 3, the pattern of the DTA curves of $KBrO_3$ systems is very similar to that of $KClO_4$ systems and evidently shows the promotion effect of additive. Jach [24] has studied the isothermal decomposition kinetics of pure $KBrO_3$ and showed that the pure bromate is able to decompose at even 342°C. In the present experiments, DTA curve 4 does not indicate such a low temperature decomposition. Joseph and Radhakrishnan Nair [25] have studied by TG method the catalytic effect on $KBrO_3$ decomposition using oxides such as Cr_2O_3, CuO, MnO_2, Al_2O_3 and TiO_2. They reported that the decomposition was kinetically analyzed by the Freeman–Carrol, Coats–Redfern and Horowitz–Metzger methods which showed a same degree of approximation to the experimental results, and that all oxides except TiO_2 catalyzed the reaction, although the mechanism of catalysis is still unknown.

Oxalates ($NiC_2O_4 \cdot 2\ H_2O$, $MgC_2O_4 \cdot 2\ H_2O$, and $CaC_2O_4 \cdot H_2O$)

The thermal decomposition of $NiC_2O_4 \cdot 2\ H_2O$ is supposed to proceed through the reactions [4,26,31]

$$NiC_2O_4 \cdot 2\ H_2O \rightarrow NiC_2O_4 + 2\ H_2O \quad (9)$$

$$NiC_2O_4 \rightarrow Ni + 2\ CO_2 \quad (10)$$

$$Ni + 0.5\ O_2 \rightarrow NiO\ (\text{in oxidative atmosphere}) \quad (11)$$

Figure 5 (curve 3) was obtained with pure $NiC_2O_4 \cdot 2\ H_2O$ in flowing N_2. Figure 6 givesthe X-ray results for samples taken out at temperatures marked with arrows (a–d) on the curve. Figure 6 shows the diffraction lines attributable to $NiC_2O_4 \cdot 2\ H_2O$ (ASTM 14-742) for sample a, anhydrous NiC_2O_4 (according to Bakcsy and Hegedus [27]), sample b, metallic Ni (ASTM 4-0850), sample c, and Ni with NiO (ASTM 4-0835) for sample d, respectively. From these results, the DTA peaks of curve 3 are found to correspond to desorption of adsorbed water near 100°C, dehydration of crystallization water at 270°C [eqn. (9)], and decomposition to Ni [eqn. (10)] at 360°C. The weak diffraction lines of NiO together with strong Ni lines in Fig. 6-d are considered to result from partial oxidation of Ni during the preparation of the sample in air for X-ray diffraction. Figure 5 (curve 1) is the DTA curve of pure $NiC_2O_4 \cdot 2\ H_2O$ in static air which shows three endothermic peaks at 130, 295, and 375°C, respectively. After the decomposition up to 800°C, X-ray analysis showed the product to be NiO alone. The small endothermic peak at 130°C may be due to the desorption of adsorbed water. α-Fe_2O_3–$NiC_2O_4 \cdot 2\ H_2O$ mixture gives the result shown by curve 2, which has a broad exothermic peak around 470°C in contrast with no exothermic peak for pure oxalate. This absence of the exotherm on curve 1 in spite of the formation of NiO is assumed to be a slow oxidation rate of Ni in static air. On the other hand, a broad exotherm at 470°C for α-Fe_2O_3–$NiC_2O_4 \cdot 2\ H_2O$ in static air (curve 2) is due to an increase in the oxidation rate. This is considered to result from the dispersion of Ni on α-Fe_2O_3 particles added which leads to good contact of Ni with air. Figure 5 (curves 4–6) shows the results in N_2 for the oxalate containing α-Fe_2O_3, CuO, and Cu_2O, respectively. The DTA pattern

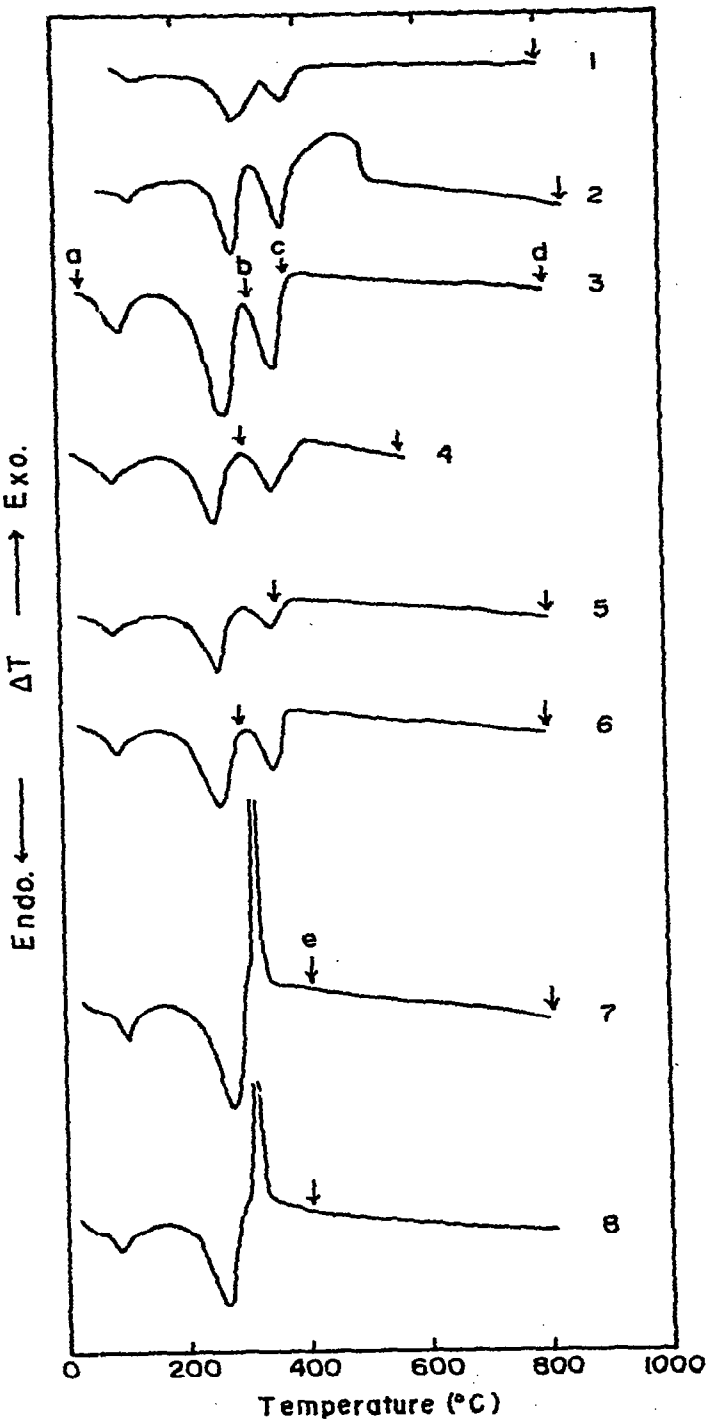

Fig. 5. DTA curves of $NiC_2O_4 \cdot 2\,H_2O$ systems. (1) $NiC_2O_4 \cdot 2\,H_2O$ in static air, (2) $NiC_2O_4 \cdot 2\,H_2O + \alpha\text{-}Fe_2O_3$ in static air, (3) $NiC_2O_4 \cdot 2\,H_2O$ in flowing N_2 (50 ml min^{-1}), (4) $NiC_2O_4 \cdot 2\,H_2O + \alpha\text{-}Fe_2O_3$ in flowing N_2, (5) $NiC_2O_4 \cdot 2\,H_2O + CuO$ in flowing N_2, (6) $NiC_2O_4 \cdot 2\,H_2O + Cu_2O$ in flowing N_2, (7) $NiC_2O_4 \cdot 2\,H_2O$ in flowing O_2 (50 ml min^{-1}), (8) $NiC_2O_4 \cdot 2\,H_2O + \alpha\text{-}Fe_2O_3$ in flowing O_2. Heating rate = 5°C min^{-1}; mixing ratio of sample to additive = 1 : 1 by weight. Arrows marked on the curves show temperatures at which the samples were obtained for X-ray diffraction.

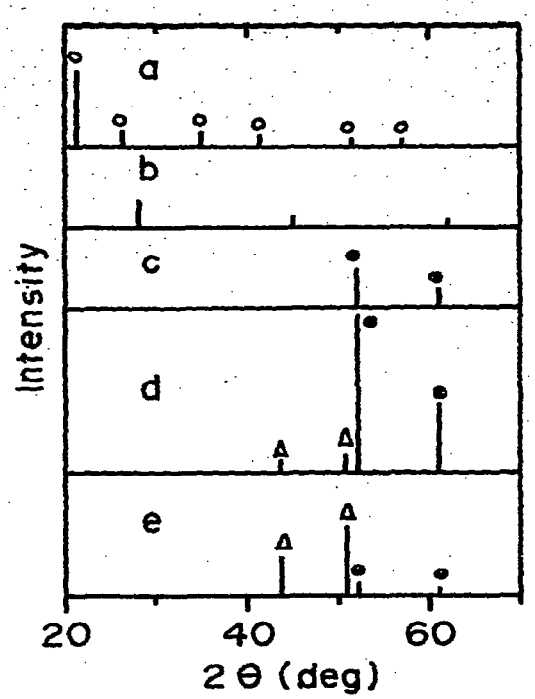

Fig. 6. X-Ray diffraction results of $NiC_2O_4 \cdot 2\,H_2O$ in the course of the decomposition in N_2 (a–d) and O_2 (e) shown in Fig. 5 (curves 3 and 7). (a) Before decomposition, (b) 315°C, (c) 375°C, (d) 805°C, (e) 410°C. (○) $NiC_2O_4 \cdot 2\,H_2O$, (●) Ni, (△) NiO, (no mark) NiC_2O_4 [27], (2θ) CoK_α.

of these curves is similar to that of pure $NiC_2O_4 \cdot 2\,H_2O$ in N_2 (curve 3). X-Ray results showed the existence of α-Fe_2O_3 at 305°C and Ni + small amount of NiO + α-Fe_2O_3 at 565°C for curve 4, CuO + Cu_2O at 353°C and NiO + Cu_2O + CuO at 805°C for curve 5, and Cu_2O at 295°C and NiO + Cu_2O + Cu at 805°C for curve 6. These facts observed in N_2 atmosphere suggest that α-Fe_2O_3 does not react with the formed Ni and copper oxides react as follows

$$Ni + 2\,CuO \rightarrow NiO + Cu_2O \quad (12)$$

$$Ni + Cu_2O \rightarrow NiO + 2\,Cu \quad (13)$$

However, these reactions could not be detected as DTA peaks. Figure 5 (curves 7 and 8) gives the DTA curves of $NiC_2O_4 \cdot 2\,H_2O$ measured in flowing O_2 atmosphere. After the endothermic dehydration of adsorbed and crystallization water at 100 and 270°C, respectively, an extremely sharp exothermic peak appears at 310°C. The sample obtained at 410°C (arrow e, curve 7) consists of NiO and Ni in small amounts as shown in Fig. 6-e. At 805°C, only NiO was formed. In the case of α-Fe_2O_3–$NiC_2O_4 \cdot 2\,H_2O$ in O_2 (curve 8), NiO, Ni (small amount) and α-Fe_2O_3 were observed at 405°C in its X-ray diffraction pattern. These facts show that the oxidation of Ni [eqn. (11)] proceeds explosively in flowing O_2. From the DTA results in Fig. 5 it is concluded that the additives do not affect the thermal decomposition of NiC_2O_4 [eqn. (10)], while the oxidation of Ni [eqn. (11)] is influenced by additives and atmosphere.

The decomposition mechanisms of NiC_2O_4 have been reported, according to Jacobs and Kureishy [28]

$$C_2O_4^{2-} \rightarrow C_2O_4 + 2\,e \tag{14a}$$

$$C_2O_4 \rightarrow 2\,CO_2 \tag{14b}$$

$$Ni^{2+} + 2\,e \rightarrow Ni \tag{14c}$$

and according to Boldyrev et al. [29]

$$C_2O_4^{2-} \rightleftharpoons 2\,CO_2^{-} \tag{15a}$$

$$2\,CO_2^{-} \rightarrow 2\,CO_2 + 2\,e \tag{15b}$$

$$Ni^{2+} + 2\,e \rightarrow Ni \tag{15c}$$

Both mechanisms contain the electron transfer step. From the fact that the semiconductive oxides, α-Fe_2O_3 (n-type), CuO and Cu_2O (p-type), did not influence the DTA behavior of the decomposition of $NiC_2O_4 \cdot 2\,H_2O$ as seen in Fig. 5, it can be presumed that the rate controlling step is eqn. (14b) or (15a) which are independent of electron transfer [30].

Figure 7 shows the DTA curves of $MgC_2O_4 \cdot 2\,H_2O$. Figure 8 shows X-ray results for samples obtained at temperatures marked by arrows (a–i) on the DTA curves. The decomposition of $MgC_2O_4 \cdot 2\,H_2O$ has been represented as [3,31,32]

$$MgC_2O_4 \cdot 2\,H_2O \rightarrow MgC_2O_4 + 2\,H_2O \tag{16}$$

$$MgC_2O_4 \rightarrow MgO + CO + CO_2 \tag{17}$$

A small endothermic peak around 100°C and a large one at 200–300°C seen on each curve in Fig. 7 correspond to the desorption of adsorbed water and the dehydration represented by eqn. (16). The thermal effect appearing between 400 and 600°C relates to the decomposition [3,31,32]. Figure 7 (curve 1) is the DTA curve of pure $MgC_2O_4 \cdot 2\,H_2O$ in static air. The sample obtained at 370°C (arrow b) shows the X-ray diffraction pattern of Fig. 8-b which is assumed to correspond to the pattern of anhydrous oxalate [3,32]. DTA curve 1 has an endotherm between 410 and 550°C which is followed by a small exothermic peak at 555°C. The sample heated up to 555°C was MgO alone (Fig. 8-c). Therefore the small exothermic peak is considered to be due to oxidation of CO formed from the decomposition [eqn. (17)] in static air [34]

$$CO + 0.5\,O_2 \rightarrow CO_2, \quad \Delta H = -283.3\ \text{kJ mole}^{-1} \tag{18}$$

As found in Fig. 8-e, α-Fe_2O_3–$MgC_2O_4 \cdot 2\,H_2O$ mixture [Fig. 7 (curve 2)] results in the formation of $MgFe_2O_4$ when it is heated up to 800°C. The area of the exothermic peak relative to that of the endothermic peak for curve 2 is larger than for curve 1. This can be explained by the promoting or catalyzing action of α-Fe_2O_3 on oxidation of CO. N_2-flowing atmosphere leads to the absence of CO oxidation or exothermic peak as indicated in Fig. 7 (curves 3 and 4). These two curves show the same DTA curve pattern, which means that α-Fe_2O_3 does not affect the decomposition reaction of eqn. (17). Fig. 8-g shows the formation of $MgFe_2O_4$ in N_2 atmosphere, but there is

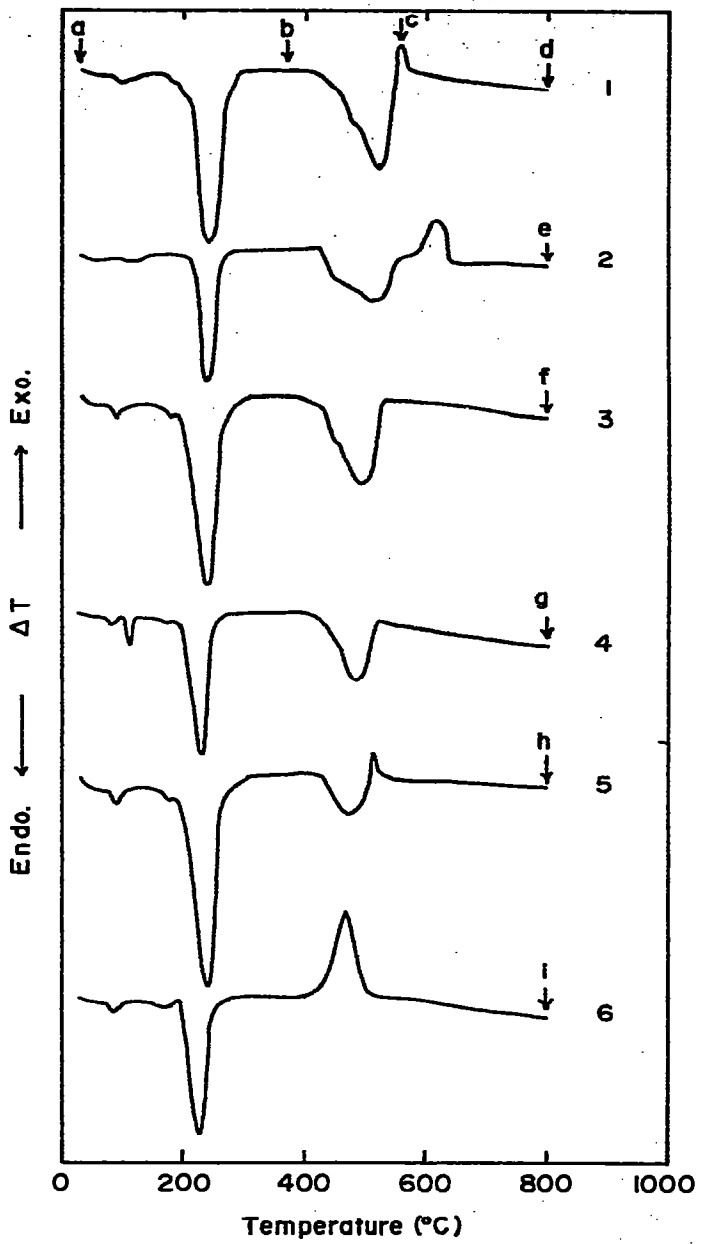

Fig. 7. DTA curves of $MgC_2O_4 \cdot 2\,H_2O$ systems. (1) $MgC_2O_4 \cdot 2\,H_2O$ in static air, (2) $MgC_2O_4 \cdot 2\,H_2O + \alpha\text{-}Fe_2O_3$ in static air, (3) $MgC_2O_4 \cdot 2\,H_2O$ in flowing N_2 (50 ml min^{-1}), (4) $MgC_2O_4 \cdot 2\,H_2O + \alpha\text{-}Fe_2O_3$ in flowing N_2, (5) $MgC_2O_4 \cdot 2\,H_2O$ in flowing O_2 (50 ml min^{-1}), (6) $MgC_2O_4 \cdot 2\,H_2O + \alpha\text{-}Fe_2O_3$ in flowing O_2. Heating rate=5°C min^{-1}; mixing ratio of sample to additive=1:1 by weight. Arrows (a–i) on the curves show temperatures at which the samples were obtained for X-ray diffraction (Fig. 8).

no change in the DTA profile of curve 4 compared with curve 3 without $MgFe_2O_4$ formation. O_2-flowing atmosphere gives DTA curves 5 and 6. Pure $MgC_2O_4 \cdot 2\,H_2O$ (curve 5) shows an endothermic peak near 480°C. The area of this peak is smaller

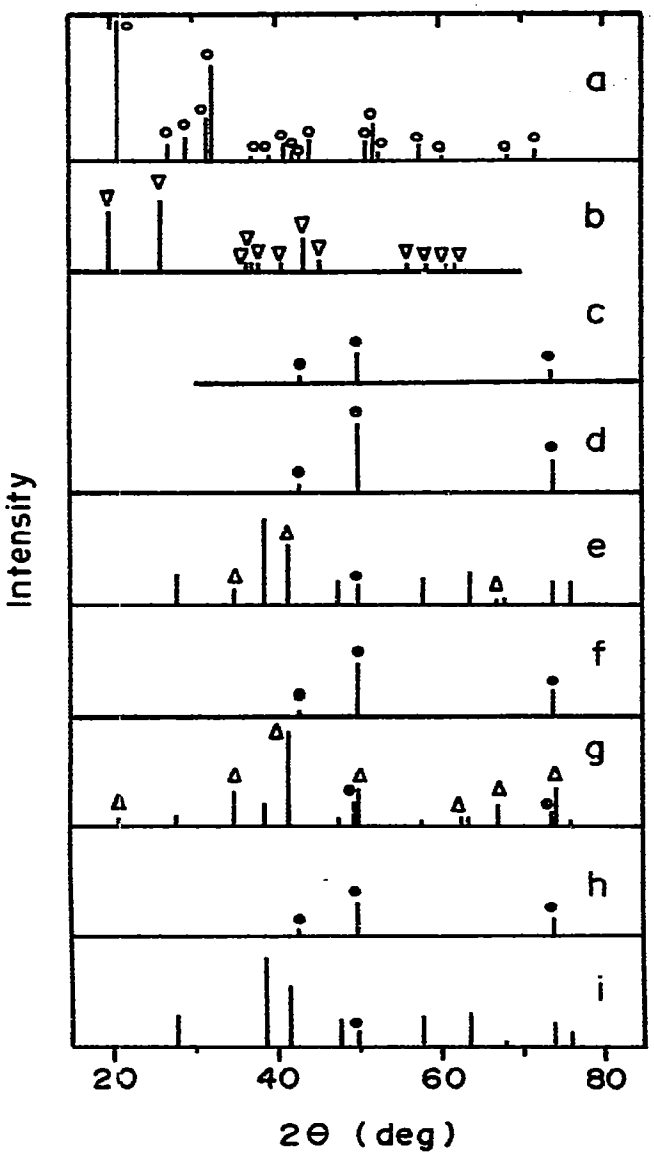

Fig. 8. X-Ray diffraction results of $MgC_2O_4 \cdot 2\,H_2O$ in the course of the decomposition in static air (a–e), N_2 (f, g) and O_2 (h, i) shown in Fig. 7. (a) Before decomposition, (b) 370°C, (c) 555°C, (d–i) 800°C. (○) $MgC_2O_4 \cdot 2\,H_2O$, (▽) MgC_2O_4, (●) MgO, (△) $MgFe_2O_4$, (no mark) α-Fe_2O_3, (2θ) CoK_α.

than that of the corresponding peak of curve 1. This may result from the difference in oxygen pressure; that is, O_2 atmosphere causes a high oxidation rate of CO simultaneously occurring with the decomposition in comparison with that in static air. Addition of α-Fe_2O_3 gives rise to only one large exothermic peak at 465°C expelling the endothermic peak as observed in curve 6. This can be attributed to both the high oxygen pressure and the catalytic action of α-Fe_2O_3 added [26]. Figure 8-i shows no formation of $MgFe_2O_4$ in O_2 atmosphere. Danforth and Dix [33] have investigated the rate of isothermal decomposition of pure MgC_2O_4 and ZnC_2O_4 in

He atmosphere by the separate measurements of volume of CO and CO_2 evolved. The proposed rate equation is

$$d\alpha/dt = k_1(1-\alpha) + k_2(1-\alpha) \quad (19)$$

where $d\alpha/dt$ is the rate and α is fraction decomposed. They concluded that the first term on the right-hand side is the rate of thermal decomposition path and the second is the rate of the path promoted or catalyzed by the decomposition product (MgO, ZnO), and that the rate controlling step for both paths is an electron transfer step

$$C_2O_4^{2-} + M^{2+} \rightarrow C_2O_4^{-} + M^{+} \quad (20)$$

Since α-Fe_2O_3 had no effect in the present DTA experiments in N_2 atmosphere [Fig. 7 (curves 3 and 4)], it was not possible to observe any promotion by the oxide added.

Figure 9 gives the results for $CaC_2O_4 \cdot H_2O$. This oxalate has been extensively investigated and used as a thermal analysis reference material. Authors have previously reported that the peak temperature of the DTA curve of $CaC_2O_4 \cdot H_2O$ strongly depends on the flow rate and the kind of gas atmosphere, and the addition of $KClO_3$ results in a singular exothermic DTA peak at 350°C [1,3,4]. The decomposition of $CaC_2O_4 \cdot H_2O$ has been represented as [34]

$$CaC_2O_4 \cdot H_2O \rightarrow CaC_2O_4 + H_2O \quad (21)$$

$$CaC_2O_4 \rightarrow CaCO_3 + CO, \quad \Delta H = 64.9 \text{ kJ mole}^{-1} \quad (22)$$

$$CaCO_3 \rightarrow CaO + CO_2, \quad \Delta H = 170.1 \text{ kJ mole}^{-1} \quad (23)$$

$$CO + 0.5\ O_2 \rightarrow CO_2, \quad \Delta H = -283.3 \text{ kJ mole}^{-1} \quad (18)$$

Table 1 contains the reaction products of $CaC_2O_4 \cdot H_2O$ systems observed by X-ray diffraction of samples obtained at temperatures marked with arrows (a–o) on DTA curves in Fig. 9. On the basis of previous investigations, the assignment of DTA peak may be as follows. The first endothermic peak at 200–260°C on each DTA curve in Fig. 9 corresponds to the dehydration of eqn. (21). The thermal effect appearing between 400 and 600°C consists of decomposition of CaC_2O_4 of eqn. (22) and oxidation of CO in oxidative atmosphere of eqn. (18). The endothermic peak above 700°C corresponds to decomposition of $CaCO_3$ [eqn. (23)]. From a comparison of peak temperatures, the temperatures for dehydration of $CaC_2O_4 \cdot H_2O$ and decomposition of $CaCO_3$ in static air (curves 1 and 2) are found to be higher than in gas-flowing atmosphere (curves 3–6) [1]. A similar temperature shift of dehydration is observed for Ni- and Mg-oxalate systems (Figs. 5 and 7). The X-ray results of Table 1 show that the final reaction product is $Ca_2Fe_2O_5$ in addition to CaO for the mixture of $CaC_2O_4 \cdot H_2O$ and α-Fe_2O_3. The formation of $Ca_2Fe_2O_5$ may be in accord with eqn. (24)

$$2\ CaO + Fe_2O_3 \rightarrow Ca_2Fe_2O_5 \quad (24)$$

On the basis of the intensity of X-ray diffraction lines, it was found that O_2 atmosphere resulted in the smallest amount of $Ca_2Fe_2O_5$. A similar tendency was seen for $MgFe_2O_4$ formation in Fig. 8. The reasons for this oxygen pressure effect is

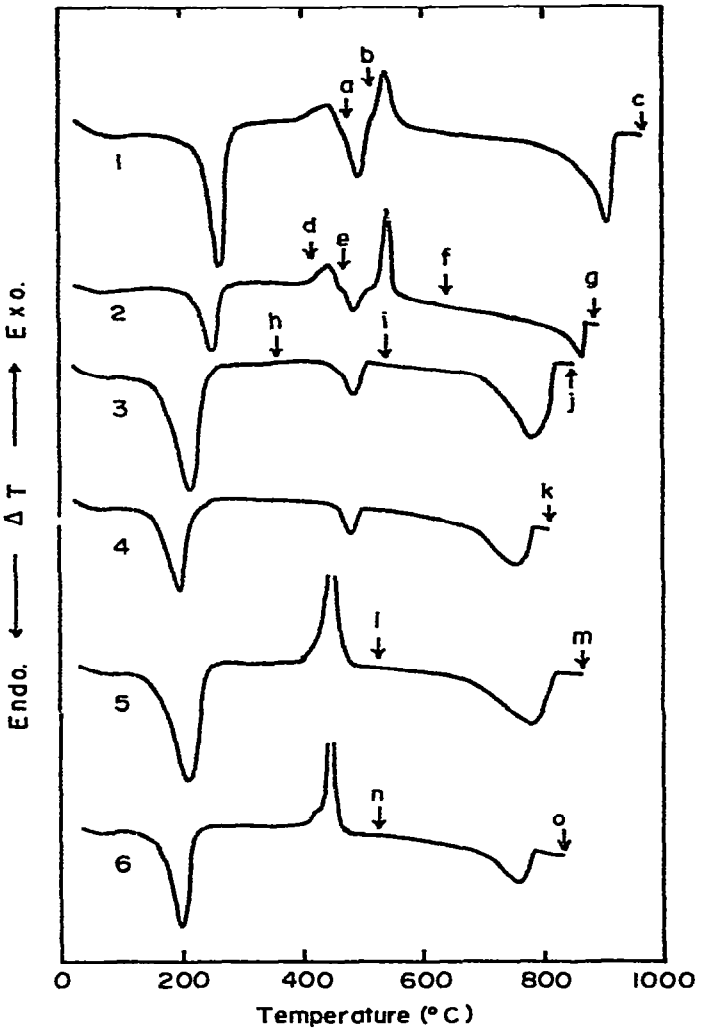

Fig. 9. DTA curves of $CaC_2O_4 \cdot H_2O$ systems. (1) $CaC_2O_4 \cdot H_2O$ in static air. (2) $CaC_2O_4 \cdot H_2O + \alpha\text{-}Fe_2O_3$ in static air. (3) $CaC_2O_4 \cdot H_2O$ in flowing N_2 (50 ml min^{-1}), (4) $CaC_2O_4 \cdot H_2O + \alpha\text{-}Fe_2O_3$ in flowing N_2, (5) $CaC_2O_4 \cdot H_2O$ in flowing O_2 (50 ml min^{-1}), (6) $CaC_2O_4 \cdot H_2O + \alpha\text{-}Fe_2O_3$ in flowing O_2. Heating rate = 5°C min^{-1}; mixing ratio of sample to additive = 1 : 1 by weight. Arrows (a–o) on the curves show temperatures at which the samples were obtained for X-ray diffraction (Table 1).

not clear, but a speculation could be that the exothermic oxidation of CO proceeds very rapidly in the case of O_2 flowing atmosphere [Fig. 9 (curve 6, 450°C) and Fig. 7 (curve 6, 470°C)], therefore the local temperature increase by heat of the oxidation leads to a decrease in the reactivity of $\alpha\text{-}Fe_2O_3$ for $Ca_2Fe_2O_5$ formation. Figure 9 (curve 1) is the DTA result of pure $CaC_2O_4 \cdot H_2O$ in static air which, after the dehydration endothermic peak at 260°C, shows the exothermic deflection starting near 400°C followed by an endothermic peak at 490°C and by an exothermic one at 540°C. The X-ray results in Table 1 indicate the partial decomposition of CaC_2O_4 at 475°C (Fig. 9a) and the complete decomposition to $CaCO_3$ at 510°C (b). Accord-

TABLE 1

Reaction products identified by X-ray diffraction for 15 samples in the course of thermal decomposition of $CaC_2O_4 \cdot H_2O$ and $CaC_2O_4 \cdot H_2O + \alpha\text{-}Fe_2O_3$

a: (475°C) * CaC_2O_4, $CaCO_3$	d: (415°C) CaC_2O_4, $\alpha\text{-}Fe_2O_3$
b: (510°C) $CaCO_3$	e: (470°C) Fe_3O_4, CaC_2O_4, $CaCO_3$
c: (965°C) CaO	f: (640°C) $\alpha\text{-}Fe_2O_3$, $CaCO_3$
	g: (890°C) $\alpha\text{-}Fe_2O_3$, $Ca_2Fe_2O_5$, CaO
h: (360°C) CaC_2O_4	k: (810°C) Fe_3O_4, $Ca_2Fe_2O_5$
i: (540°C) $CaCO_3$	
j: (850°C) CaO	
l: (525°C) $CaCO_3$	n: (525°C) $CaCO_3$, $\alpha\text{-}Fe_2O_3$
m: (865°C) CaO	o: (835°C) $\alpha\text{-}Fe_2O_3$, CaO, $Ca_2Fe_2O_5$ (small amount)

* The letters a–o correspond to those shown in Fig. 9, and the temperature in parentheses is that at which the sample was obtained.

ingly, the thermal effect appearing at 400–600°C is a result of overlapping two reactions of eqns. (22) and (18). As seen from curve 2, $\alpha\text{-}Fe_2O_3$ relatively increases the area of exothermic peak. Since the X-ray results in Table 1 (d–g) show the formation of Fe_3O_4 at 470°C in the course of decomposition between 415 and 470°C, $\alpha\text{-}Fe_2O_3$ is found to be reduced by CO

$$3\ Fe_2O_3 + CO \rightarrow 2\ Fe_3O_4 + CO_2 \qquad (25)$$

and after the completion of CO evolution at 600°C, Fe_3O_4 is re-oxidized by air. Furthermore, curves 1 and 2 show that $\alpha\text{-}Fe_2O_3$ lowers the peak temperature from 264 to 250°C for dehydration and from 905 to 865°C for decomposition of $CaCO_3$. Figure 9 (curves 3 and 4) are DTA curves obtained in flowing N_2, in which the exothermic oxidation peak of eqn. (18) disappears. Accordingly, three endothermic peaks in N_2 atmosphere correspond to the reactions of eqns. (21), (22) and (23), respectively. The final products are CaO for pure $CaC_2O_4 \cdot H_2O$ (arrow j) and $Ca_2Fe_2O_5$ and Fe_3O_4 for $\alpha\text{-}Fe_2O_3$ mixture (k). The peak temperatures of three endothermic peaks are lowered by $\alpha\text{-}Fe_2O_3$ additive from 210 to 195°C, from 485 to 478°C, and from 780 to 760°C, respectively. In the case of $NiC_2O_4 \cdot 2\ H_2O$ and $MgC_2O_4 \cdot 2\ H_2O$ (Figs. 5 and 7), the lowering of the dehydration peak temperature was observed when $\alpha\text{-}Fe_2O_3$ was added. The peak temperature lowering by $\alpha\text{-}Fe_2O_3$ may not be a chemical effect, but a physical effect; the rigid $\alpha\text{-}Fe_2O_3$ particles mixed with the oxalate particles serve as the diluent or packings to promote the escape of product gas. Figure 9 (curves 5 and 6) gives the results in flowing O_2. The similar temperature lowering is observed for the dehydration peak from 210 to 195°C and for decomposition of $CaCO_3$ from 780 to 760°C. In O_2 atmosphere, only the exothermic peak is observed instead of the endothermic peak for decomposition of CaC_2O_4 to $CaCO_3$ [eqn. (22)] at 400–500°C, because the high oxygen pressure leads to a rapid exothermic oxidation of CO immediately after the endothermic reaction

of eqn. (22). α-Fe_2O_3 is found to give no influence on the exothermic peak. This fact indicates that the solid reaction product ($CaCO_3$) has high catalytic activity for CO oxidation [31], which is different to the case of MgC_2O_4 (solid product is MgO). It was described above that α-Fe_2O_3 in static air increases the area of the exothermic peak of curve 2 at 400–600°C relative to that of curve 1 without α-Fe_2O_3. This increase may not be the catalytic effect of α-Fe_2O_3, but the diluent effect of the oxide particles promoting convection current of static air in DTA sample quartz tube as mentioned in the case of dehydration. It is concluded that α-Fe_2O_3 additive does not exert the chemical effect on the decomposition reaction of eqn. (22). If the rate determining step is the C–C bond rupture in CaC_2O_4 [29,35], it is reasonable that the semiconductive oxide shows no effect, since the rupture does not accompany the electron transfer.

Azide (NaN_3)

Figure 10 shows DTA curves for NaN_3 in flowing N_2. As is seen, the exothermic reaction is explosive and thus the top of its DTA peak could not be measured. However, the starting temperature of the exotherm is determined by the very sharp rise of the peak; that is, 405°C for pure NaN_3, 420°C for α-Al_2O_3–NaN_3, 415°C for α-Fe_2O_3, and 420°C for NiO. Judging from these starting temperatures, the oxide additives are found to inhibit the decomposition. X-Ray analysis of α-Al_2O_3–NaN_3 mixture showed only diffraction lines of α-Al_2O_3 and none of the decomposition product (Na or Na-oxide) after the decomposition reaction. The catalytic effects of oxides added to azides have been reported for the isothermal studies on AgN_3 [36] and CsN_3 [37]. Zakharov et al. [36] found that the semiconductive oxides with large electron work function tend to show higher catalytic activity in the decomposition of AgN_6, and also found that, for example, ZnO accelerates or decelerates the reaction depending on the amount of ZnO added. Sears and Steinberg [37] concluded that in the case of CsN_3, among NiO, doped NiO (Li, Cr), ZnO and CdO, the oxide which can react with Cs metal produced (for example, $NiO + 2Cs \rightarrow Cs_2O + Ni$) strongly accelerates the decomposition of the azide. These investigators have regarded the following reactions as the rate determining steps

$$N_3^- \rightarrow N_3^0 + e \tag{26}$$

or

$$N_3^0 + N_3^0 \rightarrow 3\,N_2 \tag{27}$$

where N_3^0 is an azide radical. On the other hand, Torkar et al. [38] assumed that the rate is controlled by the step of diffusion of N_3^0 or positive hole to the surface of azide particle. In this case, the effect of semiconductive oxide could not be observed. Therefore, the results shown in Fig. 10 indicate the need for further experimental data to judge the effect of additive oxides.

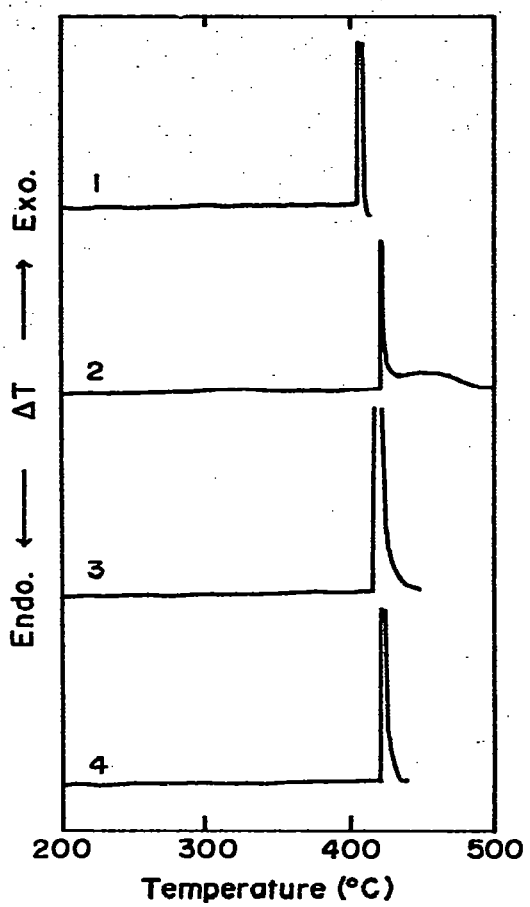

Fig. 10. DTA curves of NaN_3 systems in flowing N_2. (1) NaN_3, (2) $NaN_3 + \alpha$-Al_2O_3, (3) $NaN_3 + \alpha$-Fe_2O_3, (4) NaN_3 + NiO. Heating rate = 5°C min^{-1}; mixing ratio of NaN_3 to additive = 1.5 by weight; flowing rate of N_2 = 50 ml min^{-1}.

Permanganate ($KMnO_4$) and Oxides (MnO_2 and PbO_2)

Curves 1 and 2 in Fig. 11 show DTA results for pure $KMnO_4$ and for α-Fe_2O_3 mixture measured in flowing N_2. On the curves, an exothermic peak around 270°C and an endothermic one near 520°C are observed. The thermal decomposition processes of $KMnO_4$ are still obscure [39–43]. Figure 12-a is the X-ray diffraction pattern of sample obtained at 355°C (arrow a in Fig. 11) after the exothermic peak at 270°C. This pattern shows the disappearance of starting $KMnO_4$ and the formation of K_2MnO_4 (ASTM 12-264), but one line at $2\theta = 25°$ is unassigned. Accordingly, the exothermic peak at 270°C is found to correspond to the decomposition of $KMnO_4$ to K_2MnO_4. The stoichiometry of this decomposition may be $2\,KMnO_4 = K_2MnO_4 + MnO_2 + O_2$, but MnO_2 was not confirmed in Fig. 12-a. Addition of α-Fe_2O_3 does not give any detectable influence on the DTA pattern, but leads to a small temperature lowering of the endothermic peak from 530 to 510°C. El-Salaam and Hassan [43] reported that Fe_2O_3 prepared from iron

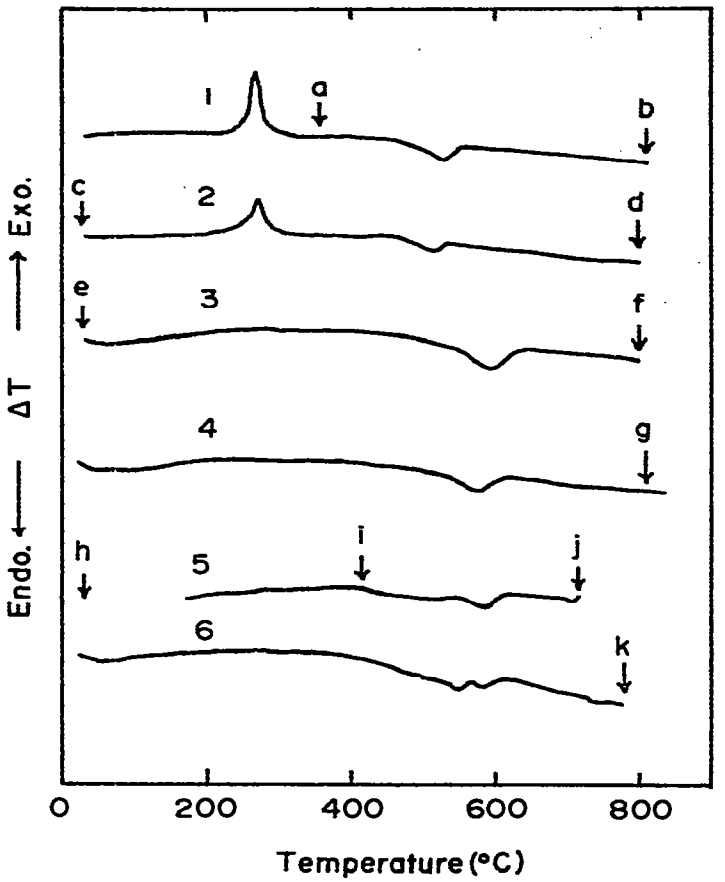

Fig. 11. DTA curves of $KMnO_4$, MnO_2 and PbO_2 in flowing N_2. (1) $KMnO_4$. (2) $KMnO_4 + \alpha$-Fe_2O_3. (3) MnO_2. (4) $MnO_2 + \alpha$-Fe_2O_3. (5) PbO_2. (6) $PbO_2 + \alpha$-Fe_2O_3. Heating rate = 5°C min^{-1}; mixing ratio of sample to additive = 1 : 1 by weight; flowing rate of N_2 = 50 ml min^{-1}. Arrows (a–k) on the curves show temperatures at which the samples were obtained for X-ray diffraction (Fig. 12).

hydroxide at 500°C gives an acceleratory effect on the decomposition of $KMnO_4$ studied with DTA and TG. Booth et al. [44] have investigated the isothermal decomposition by the use of MnO_2, ZnO and Cu_2O additives and concluded that the effectiveness of the influence of the additives relates to their prehistory and preparation. This is a similar conclusion to that of Boldyrev [41]. The endothermic peak at 520°C has been attributed to various reactions by different authors [41–43]

$$2\ MnO_2 \rightarrow Mn_2O_3 + 0.5\ O_2 \quad (28)$$

$$3\ K_2MnO_4 \rightarrow 2\ K_3MnO_4 + 0.5\ Mn_2O_3 + 1.25\ O_2 \quad (29)$$

$$10\ K_2MnO_4 \rightarrow 5.7\ K_3MnO_4 + 0.5(2.9\ K_2O \cdot 8.6\ MnO_{2.1}) + 3.4\ O_2 \quad (30)$$

The sample prepared from pure $KMnO_4$ heated up to 810°C (Fig. 11, arrow b) shows the X-ray pattern in Fig. 12-b. This pattern seems to agree with that of $K_4Mn_7O_{16}$ (pattern 1) reported by Herbstein et al. [42], but does not indicate the presence of K_3MnO_4, MnO_2 or Mn_2O_3. Accordingly, it is not possible at present to

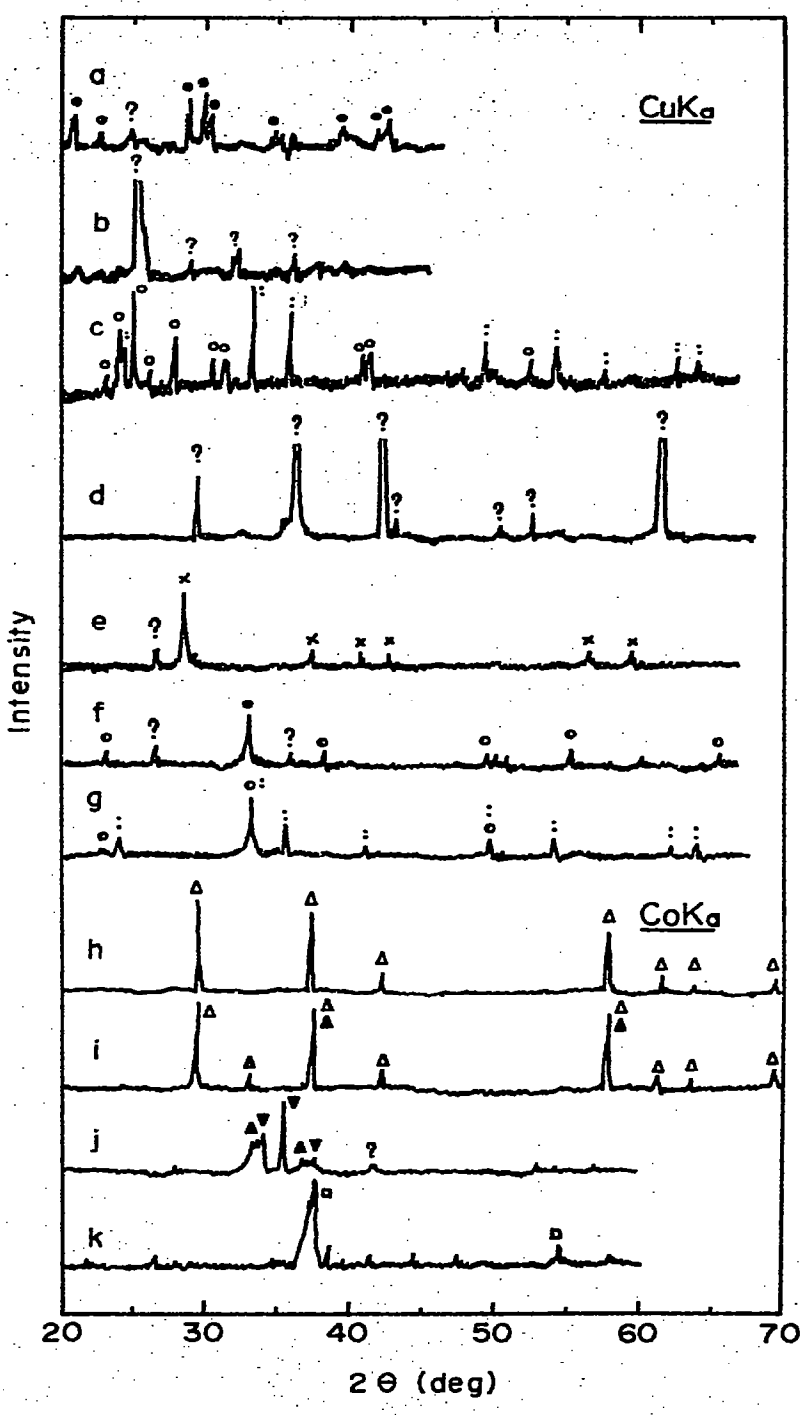

Fig. 12. X-Ray diffraction results of $KMnO_4$ (a–d), MnO_2 (e–g) and PbO_2 (h–k) systems in the course of the decomposition shown in Fig. 11. (a) 355°C, (b) 810°C, (c) before decomposition, (d) 800°C, (e) before decomposition, (f) 800°C, (g) 800°C, (h) before decomposition, (i) 415°C, (j) 715°C, (k) 780°C. (●) K_2MnO_4, (○) $KMnO_4$, (:) α-Fe_2O_3, (×) MnO_2, (◐) Mn_2O_3, (△) PbO_2, (▲) PbO (red), (▼) PbO (yellow), (□) $PbFe_2O_4$, (?) unknown.

show the reactions exactly for the endothermic peak around 520°C. Figure 12-d is the X-ray diffraction pattern of sample obtained from $KMnO_4$–α-Fe_2O_3 mixture after heating up to 800°C (Fig. 11-d). All diffraction lines are unknown. However, the lines due to α-Fe_2O_3 are completely absent, thus these unknown diffraction lines are considered to correspond to the reaction products of α-Fe_2O_3 with $KMnO_4$.

Figure 11 (curves 3 and 4) are DTA curves of MnO_2 systems. Only one endothermic peak is seen and its peak is at 595 and 575°C for pure MnO_2 and MnO_2–α-Fe_2O_3 mixture, respectively. X-Ray diffraction patterns in Fig. 12-e. f and g suggest a reaction occurred

$$2\ MnO_2 \rightarrow Mn_2O_3 + 0.5\ O_2 \tag{28}$$

and no reaction between α-Fe_2O_3 and MnO_2.

Figure 11 (curves 5 and 6) gives the results of PbO_2 systems. PbO_2 before heating gives the X-ray pattern in Fig. 12-h, which is assigned as β-PbO_2 (ASTM 11-548) or plattmerite (ASTM 8-185). On heating β-type up to 415°C (Fig. 11-i), a small amount of red PbO (ASTM 5-0561) is formed, as seen in Fig. 12-i, but the change in DTA curve is not observed in Fig. 11 (curve 5). Further heating up to 715°C (Fig. 11-j) results in yellow PbO (ASTM 5-0570) as shown in Fig. 12-j. The addition of α-Fe_2O_3 gives rise to the formation of $PbFe_2O_4$ (ASTM 4-0705) by heating the sample up to 780°C (Fig. 11-k), which is observed in Fig. 12-k. It is assumed from these X-ray results that the endothermic peak appearing at 500–600°C in Fig. 11 (curves 5 and 6) is the result of overlapping of the reactions

$$\beta\text{-}PbO_2 \rightarrow PbO\ (red) + 0.5\ O_2 \tag{31}$$

$$PbO\ (red) \rightarrow PbO\ (yellow) \tag{32}$$

$$PbO + Fe_2O_3 \rightarrow PbFe_2O_4 \tag{33}$$

The thermal decomposition of PbO_2 is reported to proceed through very complex steps [45]

$$PbO_2 \rightarrow Pb_{12}O_{19} \rightarrow Pb_{12}O_{17} \rightarrow Pb_3O_4 \rightarrow PbO \tag{34}$$

The data in Figs. 11 and 12 are still insufficient to relate the formation of $PbFe_2O_4$ to any step of eqn. (34).

REFERENCES

1 T. Ishii, K. Kamada and R. Furuichi, Kogyo Kagaku Zasshi, 74 (1971) 854.
2 S. Shimada, R. Furuichi and T. Ishii, Kogyo Kagaku Zasshi, 74 (1971) 2006.
3 T. Ishii, R. Furuichi, T. Kawasaki and K. Kamada, Bull. Fac. Eng., Hokkaido Univ., 67 (1973) 137.
4 T. Ishii, R. Furuichi and C. Okawa, Bull. Fac. Eng., Hokkaido Univ., 71 (1974) 163.
5 T. Okutani, T. Ishii and R. Furuichi, Nippon Kagaku Kaishi, (1975) 1153.
6 T. Okutani, T. Ishii and R. Furuichi, Nippon Kagaku Kaishi, (1975) 1485.
7 T. Ishii, R. Furuichi and Y. Kobayashi, Thermochim. Acta, 9 (1974) 39.
8 T. Ishii, R. Furuichi, H. Matsusato and T. Okutani, Bull. Fac. Eng., Hokkaido Univ., 89 (1978) 119.
9 R. Furuichi, T. Ishii and K. Kobayashi, J. Therm. Anal., 6 (1974) 305.
10 M. Shimokawabe, R. Furuichi and T. Ishii, Thermochim. Acta, 20 (1977) 347.

11 M. Shimokawabe, R. Furuichi and T. Ishii, Thermochim. Acta, 21 (1977) 237.
12 M. Shimokawabe, R. Furuichi and T. Ishii, Thermochim. Acta, 24 (1978) 69.
13 M.E. Brown, D. Dollimore and A.K. Galwey, in C.H. Banford and C.F.H. Tipper (Eds.), Reactions in the Solid State, Comprehensive Chemical Kinetics, Vol. 22, Elsevier, Amsterdam, 1980, p. 260.
14 R.C. Weast (Ed.), Handbook of Chemistry and Physics, CRC Press, Cleveland, OH, 51st edn., 1970.
15 W.K. Rudloff and E.S. Freeman, J. Phys. Chem., 74 (1970) 3317.
16 E.S. Freeman and W.K. Rudloff, in R.C. Mackenzie (Ed.), Differential Thermal Analysis, Vol. 1, Academic Press, New York, 1970, Chap. 12.
17 W.K. Rudloff and E.S. Freeman, J. Phys. Chem., 73 (1969) 1209.
18 M.M. Markowitz, D.A. Boryata and H. Stewart, Jr., J. Phys. Chem., 68 (1964) 2282.
19 T.W. Wydeven, J. Catal., 19 (1970) 162.
20 F. Solymosi and N. Krix, Acta Chim. Acad. Sci. Hung., 34 (1962) 241.
21 W.K. Rudloff and E.S. Freeman, J. Therm. Anal., 18 (1980) 359.
22 B.R. Phillips and D. Taylor, J. Chem. Soc., (1963) 5583.
23 J.W. Mellor, A Comprehensive Treatise on Inorganic and Theoretical Chemistry, Vol. II, Longmans, Green and Co., London, 1922, p. 407.
24 J. Jach, Proc. 4th Int. Symp. on Reactivity of Solids, 1961, p. 334, J. Phys. Chem. Solids, 24 (1963) 63, 75.
25 J. Joseph and T.D. Radhakrishnan Nair, J. Therm. Anal., 14 (1978) 271.
26 D. Dollimore, J. Therm. Anal., 11 (1977) 185.
27 Gy. Bakcsy and H.J. Hegedus, Thermochim. Acta, 10 (1974) 399.
28 P.W. Jacobs and A.R.T. Kureishy, Trans. Faraday Soc., 58 (1962) 551.
29 V.V. Boldyrev, I.S. Mevyantsev, Yu.I. Mikhailov and E.Y. Khairetdinov, Kinet. Catal. (U.S.S.R.), 11 (1970) 306.
30 L. Tournayan, H. Charcosset, H.R. Wheeler, J.M. McGinn and A.K. Galway, J. Chem. Soc. A, (1971) 868.
31 D. Dollimore and D.L. Griffiths, J. Therm. Anal., 2 (1970) 229.
32 K. Nagase, K. Sato and N. Tanaka, Bull. Chem. Soc. Jpn., 48 (1975) 437.
33 J.D. Danforth and J. Dix, J. Am. Chem. Soc., 93 (1971) 6843.
34 E.A. Simons and A.E. Newkirk, Talanta, 11 (1964) 549. O. Kubaschewski, E.L.L. Evans and C.B. Alcock, Metallurgical Thermochemistry, Pergamon Press, Oxford, 1967.
35 F.E. Freeberg, K.O. Hartman, I.C. Hisatsune and J.M. Schemph, J. Phys. Chem., 71 (1967) 397.
36 Yu.A. Zakharov, E.S. Kurochkin, G.G. Savlev and Yu.N. Rufov, Kinet. Catal., 7 (1966) 377.
37 Y. Sears and M. Steinberg, J. Catal., 11 (1968) 25.
38 K. Torkar, H.T. Spath and G.W. Herzog, in J.W. Mitchell et al. (Eds.), Proc. 6th Int. Symp. Reactivity Solids, Wiley, New York, 1969, p. 287.
39 E.G. Prout and F.C. Tompkins, Trans. Faraday Soc., 40 (1944) 488.
40 H. Peters, K.-H. Radeke and L. Till, Z. Anorg. Allg. Chem., 346 (1966) 1.
41 V.V. Boldyrev, J. Phys. Chem. Solids, 30 (1969) 1215.
42 F.H. Herbstein, G. Ron and A. Weissman, J. Chem. Soc. A, (1971) 1821; J. Chem. Soc. Dalton Trans., (1973) 1701.
43 K.M. Abp El-Salaam and E.A. Hassan, Thermochim. Acta, 38 (1980) 271.
44 J.S. Booth, D. Dollimore and G.R. Heal, Thermochim. Acta, 39 (1980) 281, 293.
45 M.I. Gillibrand and B. Halliwell, J. Inorg. Nucl. Chem., 34 (1972) 1143.